Pronounced electron-phonon interactions in ultraclean suspended carbon nanotubes

Rohan Dhall,[1] Shun-Wen Chang,[2] Zuwei Liu,[2] and Stephen B. Cronin[1,2,3,*]

[1]*Department of Electrical Engineering, University of Southern California, Los Angeles, California 90089, USA*
[2]*Department of Physics and Astronomy, University of Southern California, Los Angeles, California 90089, USA*
[3]*Department of Chemistry, University of Southern California, Los Angeles, California 90089, USA*

(Received 11 January 2012; published 18 July 2012)

We report pronounced electron-phonon interactions in suspended, nearly defect-free metallic carbon nanotubes, observed through a Kohn anomaly (KA) of greater strength than theoretically predicted. This KA is accompanied by a gate-induced modulation of the G_- band Raman intensity. By establishing a quantitative correlation between the strength of the nonadiabatic KA and the modulation of Raman intensity, we determine that the underlying cause that leads to both these effects is the same. By varying temperature, we find that metallic nanotubes can switch between a regime in which the nonadiabatic KA is clearly observed and a regime where the nonadiabatic KA is absent. The regime that does not exhibit a nonadiabatic KA is accompanied by a suppression of the Raman intensity under electrostatic gating, whereas in the regime where the nonadiabatic KA is clearly observed, strong enhancement of the Raman intensity with gating is observed.

DOI: 10.1103/PhysRevB.86.045427 PACS number(s): 73.63.Fg, 73.20.Mf, 78.67.Ch

Carbon nanotubes (CNTs) have been studied extensively over the last two decades due to their remarkable mechanical, electronic, and thermal properties. Despite this large collective body of research effort, there are still several important aspects of CNTs that are not well understood, with significant discrepancies between experiment and theory. Recently, the ability to fabricate ultraclean, nearly defect-free, suspended single-wall carbon nanotubes (SWNTs) has been developed.[1–3] This has allowed scientists to study many interesting physical phenomena such as negative differential conductance (NDC),[4] breakdown of the Born-Oppenheimer approximation,[5] Wigner crystallization,[6] Raman intensity modulation,[7] and Mott insulator behavior.[2,7] Because of their one-dimensional nature, pristine, defect-free SWNTs provide an excellent experimental platform to study the exotic physical phenomena of one-dimensional systems.

The especially strong electron-phonon coupling in this one-dimensional system has a significant effect on the G band of metallic nanotubes, which gives rise to a Kohn anomaly (KA)[8–11] and is even predicted to cause a Peierls distortion (PD) at $T = 0$ K.[12,13] The G band for metallic SWNTs consists of two peaks, a G_- peak that corresponds to the longitudinal optical (LO) phonon mode and a G_+ peak, corresponding to the transverse optical (TO) phonon mode. In metallic SWNTs, the G_- peak is downshifted and broadened due to a strong coupling of this phonon mode to the continuum of electronic states.[14] Time-dependent density functional theory (DFT) calculations predict a breakdown of the Born-Oppenheimer approximation,[15,16] which leads to the nonadiabatic KA.[17] In the nonadiabatic KA regime, the gate voltage (V_g) dependence of the G_- phonon frequency follows a W-shape profile,[15] which provides a signature of the nonadiabatic behavior.[17,18] This phenomenon has been investigated previously, both in CNTs and graphene, using Raman spectroscopy.[13,18–20] It is not surprising that the Born-Oppenheimer approximation breaks down in CNTs, given the fast vibrational motion of their tightly bound carbon atoms (0.02 ps) and long electron lifetimes (0.2–3.0 ps).[21] However, it is surprising that a vast majority of the literature on Raman spectroscopy of gated metallic CNTs shows no evidence of a nonadiabatic KA.[10,13] In these previous studies, the nanotubes were lying on a substrate and had undergone lithographic processing, which may induce defects and surface contaminants. In fact, clear nonadiabatic effects have only been observed in ultraclean, nearly defect-free, suspended CNTs.[5] This is a testament to the acute sensitivity of this one-dimensional system to perturbations from substrate interactions and surface contaminants. Furthermore, in the work presented here, the strength of this effect is found to be considerably greater than both previous experimental work and predictions made theoretically.[20,22] We have also found that nanotubes can transition between a regime in which the nonadiabatic KA is clearly evident to a second regime, where there is no sign of the nonadiabatic KA, by varying the temperature.

In this work, platinum source and drain electrodes are patterned on a $Si/SiO_2/Si_3N_4$ wafer, along with a platinum gate electrode in an 800-nm-deep, 2-μm-wide trench, as described previously.[7,18] A ferric nitrate catalyst for carbon nanotube growth is dispersed in deionized water and deposited in lithographically defined windows patterned on the source and drain electrodes. CNTs are then grown by chemical vapor deposition (CVD) using a mixture of argon gas bubbled through ethanol and hydrogen at 825 °C, yielding suspended SWNTs in a field-effect transistor (FET) geometry, as shown in Figs. 1(a) and 1(b). The nanotube growth is the final processing step in the sample fabrication, which ensures that these nanotubes are not contaminated by any chemical residues from lithographic processes. Also, since these nanotubes are suspended, there are no effects induced by the underlying substrate.

Current-bias voltage ($I - V_b$) and conductance-gate voltage ($I - V_g$) characteristics of each device are measured on a probe station in order to distinguish metallic nanotubes from semiconductors. High bias transport measurements are performed in an inert gas environment to determine whether the device is suspended, which is indicated by a region of NDC, as shown in Fig. 1(c). The value of the maximum current is used to determine whether the device is a single isolated CNT or a bundle, as established by Pop *et al.*[4] Single metallic CNTs that pass these selection criteria are selected

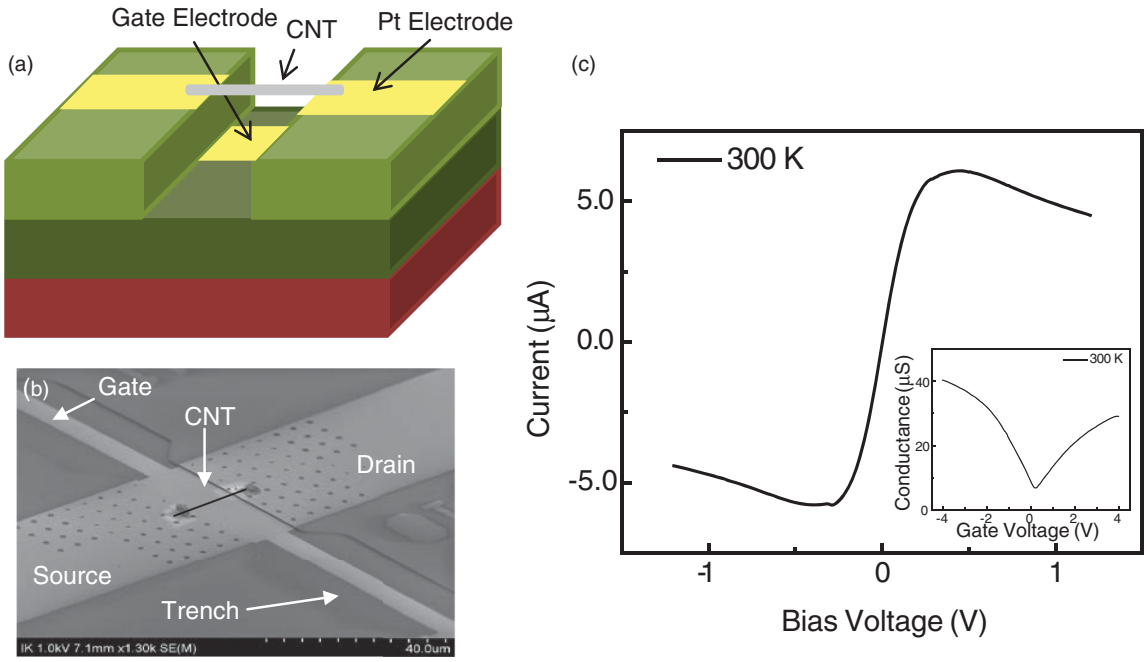

FIG. 1. (Color online) (a) Schematic diagram and (b) Scanning electron microscope (SEM) image of a suspended CNT FET device. (c) Typical room-temperature electrical current versus bias voltage characterization of a metallic SWNT. The inset shows the low-bias conductance versus gate voltage.

and wire bonded for further characterization. Raman spectra of these CNT devices are collected using either 633-nm or 532-nm wavelength radiation. The laser beam is attenuated by neutral density filters, to ensure that heating is minimal, and focused to a 1-μm spot size using a cover-glass-corrected 40× objective lens. The measurements are performed in an optical cryostat (Cryo Industries, Inc.) under vacuum at various temperatures between 4 and 400 K. As a further selection criterion, we ensure that each nanotube does not exhibit a defect-induced D-band Raman mode near 1350 cm^{-1}.[23] G_- band Raman spectra are collected at different gate voltages and fitted to both Breit-Wigner-Fano (BWF) and Lorentzian line shapes. The Raman shift, peak height, full width at half maximum (FWHM), and the electron-phonon coupling factor (Fano factor from the BWF line shape[14]) are extracted from these fits and plotted as a function of the applied gate voltage.

Figure 2 shows the G_- band Raman shift plotted as a function of the applied gate voltage, which clearly shows the W-shape profile predicted for the nonadiabatic KA (as will be seen in Fig. 7). The inset shows the raw Raman spectrum at $V_g = 0$ V. Time-dependent DFT predicts the maximum downshift in phonon frequency with gate voltage (from the ungated sample) at room temperature to be approximately 3 cm^{-1}.[15,16,20] However, as shown in Fig. 2, this device shows maximum downshifts of 15 cm^{-1} at 300 K, a stronger dependence of phonon energy on gate voltage than theoretically predicted. A similar W-shape profile has been observed in graphene but only at very low temperatures ($T = 12$ K).[24] For graphene, however, the depth of this W shape is only about 1 cm^{-1}. The significantly more pronounced W-shape profiles observed in CNTs are indicative of strong electron-phonon interaction in metallic nanotubes and of the cleanliness of suspended CNT samples fabricated in this fashion. Graphene samples, prepared on Si/SiO$_2$ substrates, are prone to spatial fluctuations of Fermi level, making it harder to observe these effects. Comparing our results with the calculations of Tsang *et al.*,[20] we conclude that the electron-phonon interaction matrix element squared is approximately 500 eV^{2}Å^{-2} for these suspended pristine metallic CNTs, which is about five times greater than values reported previously, both by experimental methods[20] and theoretical calculations.[15] For a majority of our devices, the G_- peak is significantly more intense than the G_+

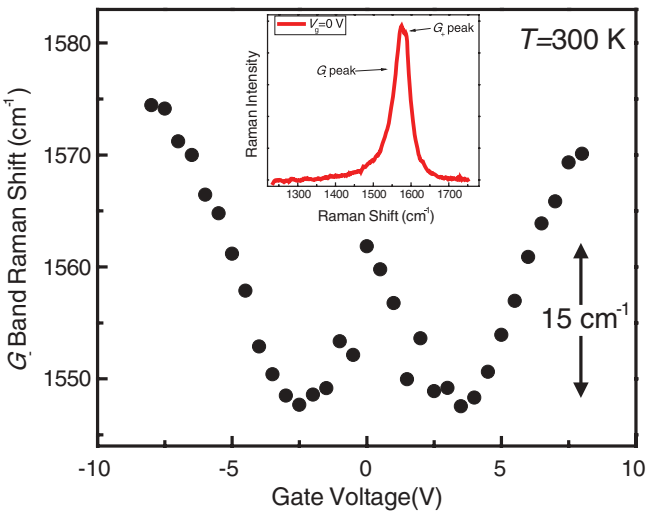

FIG. 2. (Color online) G_- band Raman shift plotted as a function of gate voltage at 300 K for sample 527-1m. The inset shows a typical Raman spectrum of a pristine metallic SWNT taken at 300 K at $V_g = 0$ V.

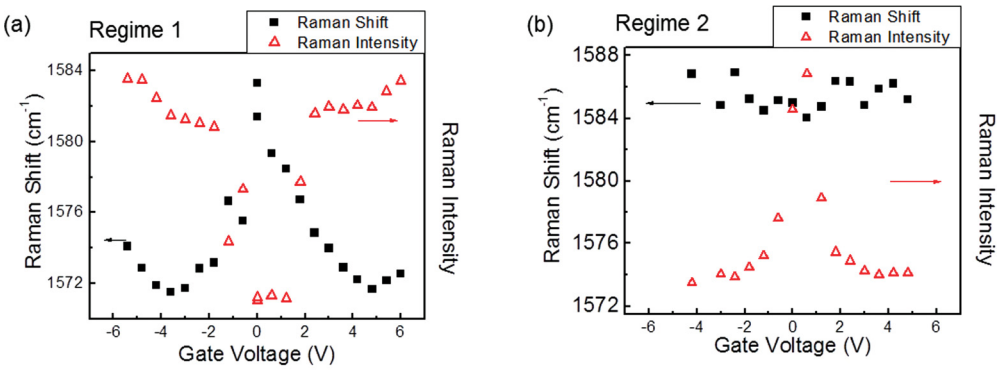

FIG. 3. (Color online) Room-temperature gate voltage dependence of the G_- band Raman shift and intensity for (a) device 435-8m, showing the signature W-shape profile indicating breakdown of the Born-Oppenheimer approximation (Regime 1) and (b) device 498-16m, showing no evidence of nonadiabatic behavior (Regime 2).

peak. Raw spectra for one such device are plotted in Figure S1 (see Supplemental Material[25]). A color plot is shown in Figure S2 (see Supplemental Material[25]), which also shows the gate dependence of the G_- band linewidth. On devices that clearly show a G_+ band, we find that the G_+ band Raman shift and intensity do not change with gate voltage.

All 25 nanotubes characterized in this study were found to exhibit only two types of behavior, which we refer to as Regime 1 and Regime 2. In Regime 1, shown in Fig. 3(a), the G-band Raman shift exhibits a strong nonadiabatic KA or W-shape profile. These devices also show a suppression of the Raman intensity near $V_g = 0$ V, as shown by the data corresponding to the right vertical axis. Not all of our samples exhibit a W-shape profile. In fact, a slight majority of samples do not exhibit this behavior. In Regime 2, shown in Fig. 3(b), no gate voltage dependence is observed in the G-band Raman shift; however, significant enhancement in the Raman intensity is observed near the charge neutrality point. Regime 1 behavior was observed in 11 of the 25 nanotubes measured in this study, showing a clear W-shape profile in the Raman shift versus V_g dependence and a gate-induced enhancement of the G-band Raman intensity. As mentioned above, this W-shape profile indicates strong electron-phonon coupling and phonon energy renormalization due to the nonadiabatic KA. The fact that this profile is not observed in Fig. 3(b) indicates that neither the KA, nor the breakdown of Born-Oppenheimer approximation, makes a significant contribution to the phonon energy renormalization in Regime 2, and the electron-phonon coupling is weak.

Interestingly, many of the devices measured in this study were found to transition from Regime 2 to Regime 1 as the temperature was lowered. Figure 4 shows the gate dependence of the G_- band for the same device measured at two different temperatures. At room temperature, the device shows no sign of the nonadiabatic KA [Fig. 4(a)], and the Raman intensity is enhanced around $V_g = 0$ V, consistent with devices in Regime 2. At 4.2 K, however, we observe the signature W-shape profile [Fig. 4(b)] and Raman intensity suppression around $V_g =$ 0 V, consistent with devices in Regime 1. It should be noted that, in the case of this particular device, the full W-shape profile cannot be seen, simply because the device was not gated strongly enough to clearly observe the upshift that follows, completing the W-shape profile. This change from 300 to 4.2 K in gate dependence was reversible and repeatable as we cooled down and warmed up the device. Hence, any contamination or damage to the nanotube can be ruled out as an underlying cause of this temperature-induced transition. Data was also collected at intermediate temperatures, and the temperature at which the device transitioned from Regime 1 to Regime 2 was found to lie between 4.2 and 100 K for device 359.

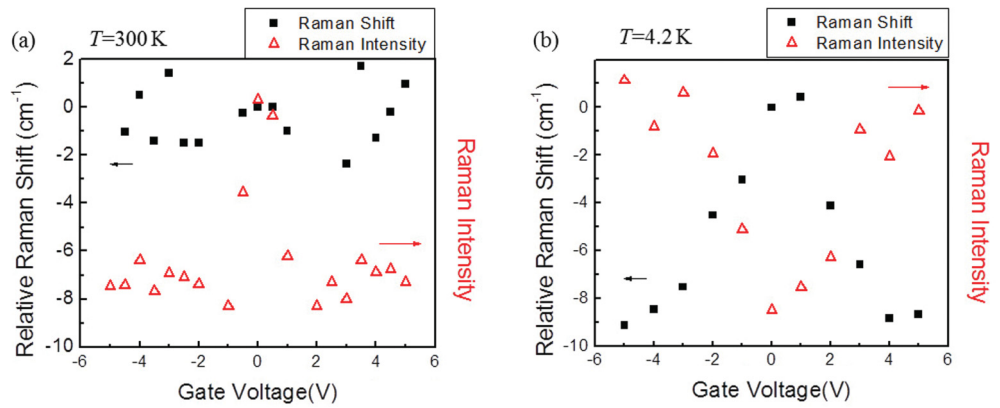

FIG. 4. (Color online) Gate voltage dependence of the G-band Raman shift and G-band Raman intensity for device 359 at (a) $T = 300$ K, consistent with Regime 2, and (b) at $T = 4.2$ K, consistent with Regime 1.

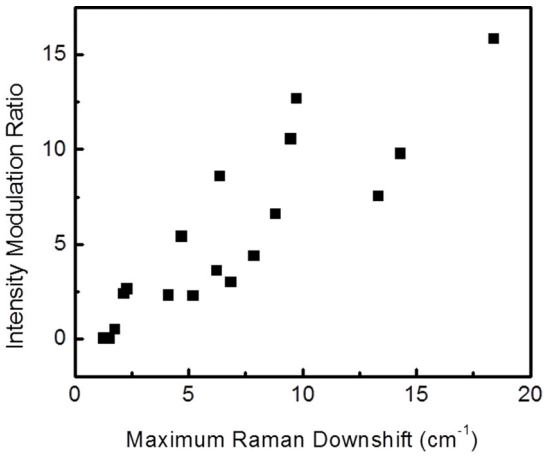

FIG. 5. Correlation between the ratio of gated and ungated G_- band Raman intensities for various devices plotted as a function of the maximum gate-induced downshift of the G_- band Raman frequency due to the nonadiabatic KA. Each point on this plot corresponds to a different nanotube sample.

These results indicate that there is a relation between the Raman intensity modulation and the nonadiabatic KA. In order to further establish this correlation, we first quantify the intensity modulation using the ratio of the Raman G-band intensities of the gated and ungated CNT. Similarly, we quantify the strength of the nonadiabatic KA from the maximum downshift observed in G-band Raman frequency from $V_g = 0$ V. This corresponds to the depth of the minima in the W-shape profile. By plotting the intensity ratio against the maximum phonon energy downshift, we obtain the linear correlation shown in Fig. 5. While both a band gap and the electronic lifetime affect nonadiabaticity, based on our limited dataset, we are unable to clearly distinguish between changes brought upon due to a band gap and due to a change in electronic lifetimes. It should be noted that, in this scheme, all the devices in Regime 2 (showing an enhanced Raman intensity around $V_g = 0$ V and no nonadiabatic KA) lie near the (0,0) point, since the Raman intensity of the doped CNT is much smaller than the undoped CNT. The G_- band linewidths for the 25 samples measured in this study spanned a wide range from 33 cm^{-1} to 83 cm^{-1}. This data is given in Table T1 in the supplementary material[25] along with the relative strengths of the nonadiabatic effects. No correlation could be established between the G_- band linewidth and either the maximum Raman downshift in the W-shape profile or the intensity modulation ratio.

The depth of the minima in the W-shape profile is directly proportional to the electron-phonon coupling matrix element, and the wide range of values obtained for this depth can be explained by the chirality dependence of electron-phonon coupling in SWNTs.[22] The linear correlation between this depth and the intensity modulation, as shown in Fig. 5, suggests that intensity modulation is a manifestation of the same underlying mechanism, i.e., electron-phonon interaction. An abrupt change in the Raman intensity, as shown in Fig. 3(a), can arise from a structural phase transition. For example, a Mott insulator transition or Peierls transition can result in a charge-density wave, which lowers the symmetry of the crystal and can change these vibrational modes from Raman active to Raman inactive, thus resulting in an abrupt drop in Raman intensity near the charge neutrality point. However, from our limited datasets, we are unable to establish exactly which instability is producing these effects, and further studies are needed in this direction.

The minima in the W-shape profile have been predicted to deepen significantly as the temperature is lowered for graphene and metallic CNTs.[15,20,22] These calculations assume linear bands for electron dispersion, with no band gap. This general trend is observed on several devices, although, the effect is still not as pronounced as theoretically predicted. For a significant fraction of our devices, however, we do not see this trend. Figure 6 shows the gate dependence of the G_- band Raman shift relative to the Raman shift at $V_g = 0$, at different temperatures for two different CNT devices. Both devices show the W-shape profile, indicating a strong nonadiabatic KA. However, at low temperatures, the device in Fig. 6(a) clearly shows a deepening of the minima in Raman shift. In contrast, for a number of other devices, such as the one shown in Fig. 6(b), we saw no appreciable change in the gate dependence of the Raman shift at different temperatures.

The KA occurs in metallic CNTs when a phonon excites an electron-hole pair across the tiny band gap of the metal.[15] The creation of this electron-hole pair renormalizes the phonon self-energy. A renormalized phonon self-energy is written

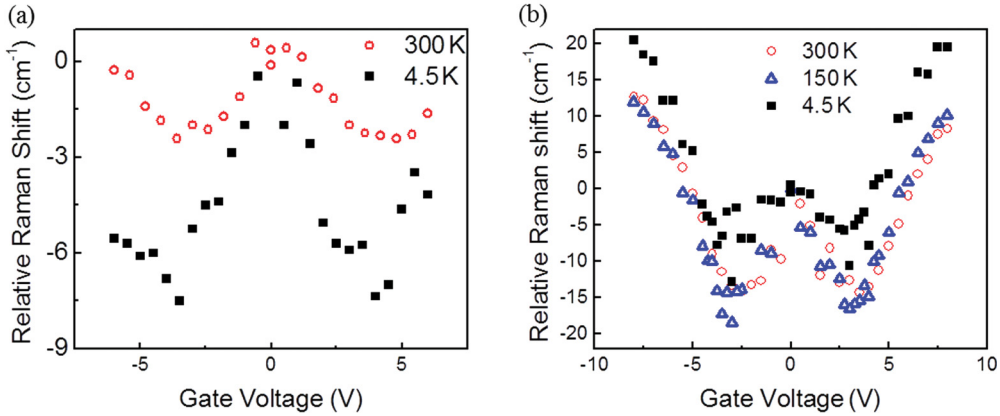

FIG. 6. (Color online) Relative Raman shift of the G_- band with respect to $V_g = 0$ for (a) device 491-15 and (b) device 527-1 taken at various temperatures.

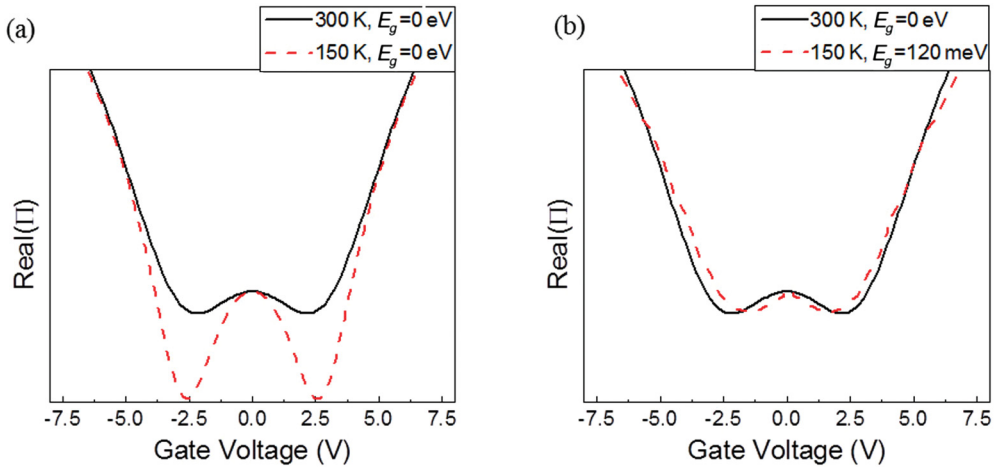

FIG. 7. (Color online) The real part of $\Pi(\omega, E_F)$ from Eq. (1) at $T = 300$ K and $T = 150$ K, with (a) no band gap in the electron band structure and (b) a band gap of 120 meV.

as the sum of the unrenormalized energy, $\hbar\omega$, and the real part of the phonon self-energy, $\Pi(\omega, E_F)$. The imaginary part of this self-energy gives the phonon lifetime and hence the width of the phonon mode. From second-order time-dependent perturbation theory, the self-energy is given as

$$\Pi(\omega, E_F) = 2\sum_{\mathbf{k}}\left(\frac{|V_{\mathbf{k}}|^2}{\hbar\omega - E^{eh}_{\mathbf{k}} + i\Gamma/2} - \frac{|V_{\mathbf{k}}|^2}{\hbar\omega + E^{eh}_{\mathbf{k}} + i\Gamma/2}\right) \times (f_h - f_e), \quad (1)$$

where the prefactor 2 comes from spin degeneracy.[22] Here, $f_{h,e}$ are the Fermi distribution functions for holes and electrons, $E^{eh}_{\mathbf{k}} = E^{e}_{\mathbf{k}} - E^{h}_{\mathbf{k}}$, where $E^{e}_{\mathbf{k}}$ ($E^{h}_{\mathbf{k}}$) is the electron (hole) energy and $V_{\mathbf{k}}$ is the electron-phonon matrix element that converts a phonon into an electron-hole pair. By doping the nanotube, we increase its Fermi energy so that states in the conduction band are occupied. At $T = 0$ K, when $E_F = \frac{\hbar\omega}{2}$, all the electronic states that can be excited by a phonon are occupied, which switches off the KA and dramatically changes the electronic screening of phonons. As a result, this phonon renormalization is extremely sensitive to the band gap of the nanotube. Since metallic nanotubes actually have nonzero band gaps, we must consider a model that includes the finite effective mass of the electrons. Using a finite-mass Dirac dispersion relation ($E = \sqrt{m^2 + (\hbar\upsilon_F k)^2}$) in the nonadiabatic case at $T = 0$, we obtain

$$\mathrm{Re}\left[\Pi(\omega, E_F)\right] = \frac{-\alpha}{2}\left[E_C - E_F - \left\{\frac{(\hbar\omega)^2 - (2m)^2}{4\hbar\omega}\right\} \ln\left|\frac{|E_F| - \frac{\hbar\omega}{2}}{|E_F| + \frac{\hbar\omega}{2}}\right|\right], \quad (2)$$

where α and E_C are constants and $2m$ is the band gap.[22] In this case, we see that the logarithmic singularity can be eliminated if the band gap nears the phonon energy, thus explaining why some nanotubes do not show a strengthening of the KA at lower temperatures, as in Fig. 6(b). In order to more accurately interpret the experimental observations presented in this study, both the functional form of the matrix element, $V_{\mathbf{k}}$, and the curvature induced minigap must be considered. Unfortunately, this requires a precise knowledge of the nanotube chirality.

According to Engelsberg and Schrieffer,[26] nonadiabatic phonon frequencies are observed when the electronic momentum relaxation is slower than the phonon frequency. One can, thus, switch from adiabatic to nonadiabatic frequencies by changing the electronic relaxation time [that is, by changing the parameter Γ in Eq. (1)]. The observed transition away from nonadiabatic behavior, as shown in Fig. 5, is brought upon by varying the temperature only. While the underlying nature of this change is not fully illuminated by this data, one possibility is that the electron lifetime (and hence Γ) changes with temperature. However, if that is the case, one expects to see a monotonic phonon hardening, as reported by Farhat *et al.*[10] The fact that this is not observed in our experiment indicates that the change in behavior is due to a change in the electron-phonon interaction matrix element, $V_{\mathbf{k}}$. This is further corroborated by the observed G_- band linewidths at different temperatures, which do not change considerably.

Figure 7(a) shows the calculated real part of the phonon self-energy [based on Eq. (1)] plotted as a function of the applied gate voltage, for two different temperatures, assuming there is no band gap in the electron band structure of the metallic CNT. In this case, we can clearly see a deepening of the minima in the W-shape profile, which has been reported previously.[11,15,20] This behavior agrees with the trend observed in Fig. 6(a). However, the inclusion of a miniband gap (120 meV) at $T = 150$ K in the band structure of the CNT, can reduce the renormalization of phonon energy, as shown in Fig. 7(b). Small band gaps of $\sim$100 meV ($\gg k_B T$) have been observed experimentally in metallic nanotubes[2,7] and have been attributed to the effect of curvature[22] and electron-electron interactions.[2] These calculations indicate that the experimental data shown in Fig. 6(b) can be explained if a band gap opens up in the metallic CNT as the temperature is lowered.[7] The electron-phonon coupling matrix element, $|V_{\mathbf{k}}|$, is assumed to be the same for all cases in Fig. 7. One must note, however, that these calculations involve several simplifications, making it difficult to provide an exact estimate for the electron-phonon interaction from our experimental data. Ideally, the electron-phonon matrix element, $V_{\mathbf{k}}$, depends on the electron wavevector $\mathbf{k}$. In a more

detailed analysis, one could calculate the electron and hole wave functions using an extended tight binding model[27] and thereby obtain the bare electron-phonon matrix element (g), using a deformation potential form of interaction.[22,28,29] Given the nanotube chirality, it is then possible to assign a functional form to the $\mathbf{k}$ dependence of $V_{\mathbf{k}}$, which is proportional to g. However this simplification qualitatively captures the physical understanding of how a band-gap influences the phonon renormalization.[20] A more rigorous analysis would require information about the chirality of the nanotube to precisely calculate this matrix element, since the functional form of $V_{\mathbf{k}}$ varies with chirality. Unfortunately, none of the nanotubes presented in this study exhibited a radial breathing mode. We were, therefore, unable to identify the chirality of the nanotubes, and this issue is yet to be investigated experimentally.

As mentioned above, the W-shape profiles observed in this work, and hence electron-phonon interaction matrix elements, are significantly larger than values reported previously, both by experimental methods[20] and theoretical calculations.[15] A recent study of graphene has indicated that the presence of long-range electron-electron interactions renormalize both the phonon dispersion curve and the strength of the electron-phonon coupling matrix element using more accurate calculations of the electron band structure through the GW approximation.[30] The electron-phonon coupling matrix element calculated in this manner was found to be about 50% larger than the value obtained using the local-density approximation. In view of this result, we feel similar theoretical studies are needed for metallic SWNTs to explore the role electron-electron interactions may have in enhancing the electron-phonon interaction and possible structural phase change.

In conclusion, the immense strength of the electron-phonon interactions in metallic CNTs causes their phonon energies to depend strongly on the free-carrier density. We find that these pristine nanotubes exist in one of two regimes—(1) having no sign of the breakdown of the Born-Oppenheimer approximation and showing a suppression of the G_- band Raman intensity with electrostatic gating and (2) showing a breakdown of the adiabatic approximation and accompanied by a dramatic gate-induced enhancement of G_- band Raman intensity. We establish that the coupling between electrons and phonons in metallic CNTs is approximately five times stronger than previous theoretical and experimental reports and that the strength of this coupling is correlated with the gate-induced Raman intensity modulation. The abrupt changes in the Raman intensity can arise from a structural phase transition, (e.g., charge-density wave), which lowers the symmetry of the crystal, and can change these vibrational modes from Raman active to Raman inactive. We feel that, in light of this evidence, the electron-phonon interactions in metallic CNTs should be theoretically reexamined.

This research was supported in part by ONR Award No. N000141010511, DOE Award No. DE-FG02-07ER46376, and NSF Award No. CBET-0854118. A portion of this work was done in the UCSB nanofabrication facility, part of the NSF-funded NNIN network.

*Corresponding author: scronin@usc.edu

[1] Z. Yao, C. L. Kane, and C. Dekker, Phys. Rev. Lett. **84**, 2941 (2000).
[2] V. V. Deshpande, B. Chandra, R. Caldwell, D. S. Novikov, J. Hone, and M. Bockrath, Science **323**, 106 (2009).
[3] J. Cao, Q. Wang, and H. Dai, Nat. Mater. **4**, 745 (2005).
[4] E. Pop, D. Mann, J. Cao, Q. Wang, K. Goodson, and H. Dai, Phys. Rev. Lett. **95**, 155505 (2005).
[5] A. W. Bushmaker, V. V. Deshpande, S. Hsieh, M. W. Bockrath, and S. B. Cronin, Nano Lett. **9**, 607 (2009).
[6] V. V. Deshpande and M. Bockrath, Nat. Phys. **4**, 314 (2008).
[7] A. W. Bushmaker, V. V. Deshpande, S. Hsieh, M. W. Bockrath, and S. B. Cronin, Phys. Rev. Lett. **103**, 67401 (2009).
[8] M. Lazzeri and F. Mauri, Phys. Rev. Lett. **97**, 266407 (2006).
[9] W. Kohn, Phys. Rev. Lett. **2**, 393 (1959).
[10] H. Farhat, H. Son, G. G. Samsonidze, S. Reich, M. Dresselhaus, and J. Kong, Phys. Rev. Lett. **99**, 145506 (2007).
[11] R. Barnett, E. Demler, and E. Kaxiras, Phys. Rev. B **71**, 035429 (2005).
[12] J. Maultzsch, S. Reich, U. Schlecht, and C. Thomsen, Phys. Rev. Lett. **91**, 087402 (2003).
[13] P. M. Rafailov, J. Maultzsch, C. Thomsen, and H. Kataura, Phys. Rev. B **72**, 045411 (2005).
[14] S. Brown, A. Jorio, P. Corio, M. Dresselhaus, G. Dresselhaus, R. Saito, and K. Kneipp, Phys. Rev. B **63**, 155414 (2001).
[15] S. Piscanec, M. Lazzeri, J. Robertson, A. C. Ferrari, and F. Mauri, Phys. Rev. B **75**, 035427 (2007).
[16] K. Ishikawa and T. Ando, J. Phys. Soc. Jpn. **75**, 4713 (2006).
[17] N. Caudal, A. M. Saitta, M. Lazzeri, and F. Mauri, Phys. Rev. B **75**, 115423 (2007).
[18] A. W. Bushmaker, V. V. Deshpande, S. Hsieh, M. W. Bockrath, and S. B. Cronin, Nano Lett. **9**, 607 (2009).
[19] S. Pisana, M. Lazzeri, C. Casiraghi, K. S. Novoselov, A. K. Geim, A. C. Ferrari, and F. Mauri, Nat. Mater. **6**, 198 (2007).
[20] J. Tsang, M. Freitag, V. Perebeinos, J. Liu, and P. Avouris, Nat. Nanotechnol. **2**, 725 (2007).
[21] J. Y. Park, S. Rosenblatt, Y. Yaish, V. Sazonova, H. Üstünel, S. Braig, T. Arias, P. W. Brouwer, and P. L. McEuen, Nano Lett. **4**, 517 (2004).
[22] K. Sasaki, H. Farhat, R. Saito, and M. S. Dresselhaus, Physica E **42**, 2005 (2010).
[23] A. Jorio, M. Pimenta, A. Souza Filho, R. Saito, G. Dresselhaus, and M. Dresselhaus, New J. Phys. **5**, 139 (2003).
[24] J. Yan, E. A. Henriksen, P. Kim, and A. Pinczuk, Phys. Rev. Lett. **101**, 136804 (2008).
[25] See Supplemental Material at http://link.aps.org/supplemental/10.1103/PhysRevB.86.045427 for additional data.
[26] S. Engelsberg and J. Schrieffer, Phys. Rev. **131**, 993 (1963).
[27] G. G. Samsonidze, R. Saito, N. Kobayashi, A. Grüneis, J. Jiang, A. Jorio, S. Chou, G. Dresselhaus, and M. Dresselhaus, Appl. Phys. Lett. **85**, 5703 (2004).
[28] J. Jiang, R. Saito, G. G. Samsonidze, S. Chou, A. Jorio, G. Dresselhaus, and M. Dresselhaus, Phys. Rev. B **72**, 235408 (2005).
[29] D. Porezag, T. Frauenheim, T. Köhler, G. Seifert, and R. Kaschner, Phys. Rev. B **51**, 12947 (1995).
[30] M. Lazzeri, C. Attaccalite, L. Wirtz, and F. Mauri, Phys. Rev. B **78**, 081406 (2008).